

4-2020

Estimation of Aboveground Biomass of *Robinia pseudoacacia* Forest in the Yellow River Delta based on UAV and Backpack LiDAR Point Clouds

Jinbo Lu
Hohai University

Hong Wang
Hohai University

Shuhong Qin
Hohai University

Lin Cao
Nanjing Forestry University

Ruiliang Pu
University of South Florida, rpu@usf.edu

See next page for additional authors
Follow this and additional works at: https://digitalcommons.usf.edu/geo_facpub

 Part of the [Earth Sciences Commons](#)

Scholar Commons Citation

Lu, Jinbo; Wang, Hong; Qin, Shuhong; Cao, Lin; Pu, Ruiliang; Li, Guilin; and Sun, Jing, "Estimation of Aboveground Biomass of *Robinia pseudoacacia* Forest in the Yellow River Delta based on UAV and Backpack LiDAR Point Clouds" (2020). *School of Geosciences Faculty and Staff Publications*. 2263. https://digitalcommons.usf.edu/geo_facpub/2263

This Article is brought to you for free and open access by the School of Geosciences at Digital Commons @ University of South Florida. It has been accepted for inclusion in School of Geosciences Faculty and Staff Publications by an authorized administrator of Digital Commons @ University of South Florida. For more information, please contact digitalcommons@usf.edu.

Authors

Jinbo Lu, Hong Wang, Shuhong Qin, Lin Cao, Ruiliang Pu, Guilin Li, and Jing Sun



Estimation of aboveground biomass of *Robinia pseudoacacia* forest in the Yellow River Delta based on UAV and Backpack LiDAR point clouds

Jinbo Lu^a, Hong Wang^{a,*}, Shuhong Qin^a, Lin Cao^b, Ruiliang Pu^c, Guilin Li^a, Jing Sun^a

^a School of Earth Science and Engineering, Hohai University, Fo Cheng Xi Road 8, Nanjing, 211100, China

^b Co-Innovation Center for Sustainable Forestry in Southern China, Nanjing Forestry University, Nanjing, 210037, China

^c School of Geosciences, University of South Florida, 4202 E. Fowler Avenue, NES 107, Tampa, FL, 33620, USA

ARTICLE INFO

Keywords:

UAV-LiDAR
Backpack-LiDAR
Individual tree segmentation
Forest AGB
The Yellow River Delta

ABSTRACT

Forest plantations are an important source of terrestrial carbon sequestration. The forest of *Robinia pseudoacacia* in the Yellow River Delta (YRD) is the largest artificial ecological protection forest in China. However, more than half of the forest has appeared different degrees of dieback and even death since the 1990s. Timely and accurate estimation of the forest aboveground biomass (AGB) is a basis for studying the carbon cycle of forests. Light Detecting and Ranging (LiDAR) has been proved to be one of the most powerful methods for forest biomass estimation. However, because of an irregular and overlapping shape of the broadleaved forest canopy in a growing season, it is difficult to segment individual trees and estimate the tree biomass from airborne LiDAR data. In this study, a new method was proposed to solve this problem of individual tree detection in the *Robinia pseudoacacia* forest based on a combination of the Unmanned Aerial Vehicle-Light Detecting and Ranging (UAV-LiDAR) with the Backpack-LiDAR. The proposed method mainly consists of following steps: (i) at a plot level, trees in the UAV-LiDAR data were detected by seed points obtained by an individual tree segmentation (ITS) method from the Backpack-LiDAR data; (ii) height and diameter at breast height (DBH) of an individual tree would be extracted from UAV and Backpack LiDAR data, respectively; (iii) the individual tree AGB would be calculated through an allometric equation and the forest AGB at the plot level was accumulated; and (iv) the plot-level forest AGB was taken as a dependent variable, and various metrics extracted from UAV-LiDAR point cloud data as independent variables to estimate forest AGB distribution in the study area by using both multiple linear regression (MLR) and random forest (RF) models. The results demonstrate that: (1) the seed points extracted from Backpack-LiDAR could significantly improve the overall accuracy of individual tree detection ($F = 0.99$), and thus increase the forest AGB estimation accuracy; (2) compared with MLR model, the RF model led to a higher estimation accuracy ($p < 0.05$); and (3) LiDAR intensity information selected by both MLR and RF models and laser penetration rate (LP) played an important role in estimating healthy forest AGB.

1. Introduction

Artificial afforestation is considered to be one of the most ecologically effective ways to increase carbon sequestration by absorbing CO₂ and mitigating climate warming (Piao et al., 2009). China has carried out a wide range of ecological projects such as forest protection and afforestation. The artificial forest area in China accounts for 73 % of the global artificial forest area, which has become an important means of increasing China's terrestrial carbon sequestration (Zhou et al., 2012). The Yellow River Delta (YRD) has the largest area of artificial *Robinia pseudoacacia* forest in China. Due to low soil fertility and widespread soil salinization, there are no natural forests in the YRD. The *Robinia*

pseudoacacia forest, with characteristics of strong adaptability, drought and certain salt tolerance, has been widely planted since the 1970s. However, nearly 60 % of *Robinia pseudoacacia* forests has suffered from different degrees of dieback and even death (Wang et al., 2015a). Timely and accurate estimation of *Robinia pseudoacacia* forest above ground biomass (AGB) can provide a scientific basis for assessing forest plantation carbon sinks in the YRD.

Measuring forest biomass through field survey at a large spatial scale is time consuming and cost-expensive, and thus is difficult to popularize (Hermosilla et al., 2014; Van Leeuwen and Nieuwenhuis, 2010). Remote sensing technology, such as Light Detection and Ranging (LiDAR), has proved its potential of providing detailed characteristics of

* Corresponding author.

E-mail addresses: jinbo@hhu.edu.cn (J. Lu), hongwang@hhu.edu.cn (H. Wang), qinshuhong@hhu.edu.cn (S. Qin), lincao@njfu.edu.cn (L. Cao), rpu@usf.edu (R. Pu), liguimumu@163.com (G. Li), sunjing@hhu.edu.cn (J. Sun).

<https://doi.org/10.1016/j.jag.2019.102014>

Received 24 July 2019; Received in revised form 12 October 2019; Accepted 12 November 2019

Available online 24 November 2019

0303-2434/ © 2019 Elsevier B.V. This is an open access article under the CC BY-NC-ND license (<http://creativecommons.org/licenses/by-nc-nd/4.0/>).

forest canopy structure in three-dimensions (Lefsky et al., 2002; Næsset and Gobakken, 2008). The forest height with sub-meter vertical precision and horizontal distribution information can be extracted from LiDAR data, which has significant advantages in forest AGB estimation (e.g., Cao et al., 2016; Hudak et al., 2012).

The individual tree segmentation (ITS) is of great significance in forest AGB estimation from LiDAR data. Once trees are accurately segmented, the tree structure parameters, such as tree height and crown diameter, can be directly extracted at a high precision (Solberg et al., 2006). Then forest AGB can be accurately estimated using an allometric equation (Basuki et al., 2009; Wang, 2006). The LiDAR data derived ITS uses either point cloud data directly or canopy height model (CHM) derived from the point cloud data (Liu et al., 2019; Zhen et al., 2016). CHM-based segmentation uses the first echo of laser point cloud only and is impractical for the detection of understory trees. Therefore, the point-based segmentation has been rapidly developed in recent years. For examples, Reitberger et al. (2009) used the random sample consensus algorithm to detect individual tree trunks with an accuracy of near 70 %. According to characteristics of the crown spacing of coniferous trees being larger than the understory, Li et al. (2012) took the top laser point cloud from a tree crown as seed points to separate individual trees based on the top-to-down regional growth method, achieving a total accuracy of 90 %. However, when this method was applied to broadleaved forests, the accuracy was reduced. Since the broadleaved forest canopy is irregular in shape with crossed and overlapped branches and leaves, it is difficult to determine seed points from the crown top with point cloud data. Lu et al. (2014) used the intensity information from LiDAR point cloud data acquired in a deciduous season and extracted a topological relationship between a trunk and the point cloud to segment the trunk, and they achieved a total accuracy of 90 %. However, this method can only be applied in the deciduous season. This is because, in a growing season, the leaf intensity value is also very large, which interferes with an extraction process of the trunk.

Regional AGB estimation based on LiDAR data is usually obtained by establishing a model between characteristic variables extracted from LiDAR sample data and forest inventory attributes. The height and density variables extracted from LiDAR point cloud data have been proved to be strongly correlated with forest biomass (Hall et al., 2005; Næsset and Gobakken, 2008). However, only using LiDAR metrics of the forest height and density information is insufficient to describe an overall canopy layer and heterogeneity vertically, and thus Zhang et al. (2017) added a canopy height distribution (Weishampel et al., 2007; Zhao et al., 2009) and branch and leaf profile (Lovell et al., 2003), which describe characteristic variables of the canopy profile, and they used a Weibull function to fit parameters to infer the broadleaved forest AGB resulting in a good result ($R^2 = 0.66$, $RMSE = 26.67$ Mg/ha). Although the first echo of laser point cloud provides information on the upper canopy structure, the last echo distribution describes the maximum penetrating laser signal in the vegetation layer, which can distinguish forest types with different degrees of degradation and improve the estimation accuracy of biomass (Ioki et al., 2014). Since single-spectrum LiDAR sensors typically use 1064 nm near-infrared wavelength, which is well-suited for identifying changes in plant reflectivity, the healthy trees usually have strong backscattering (Lorenzen and Jensen, 1988). Yoga et al. (2017) used remote sensing images and intensity information extracted from LiDAR to eliminate dead trees identified by a random forest model classification and got an improved estimation accuracy of forest stocks. Therefore, the height metrics, density metrics, profile characteristic metrics, last echo transmittance, and intensity information extracted from LiDAR data all have been proved to be useful characteristic variables for forest AGB estimation.

Unmanned Aerial Vehicle (UAV) systems represent a low-cost, agile, and autonomous opportunity, and thus make them an alternative platform to satellites and aircrafts for forest inventory (Dandois et al., 2015; Sankey et al., 2017). It has been proved that UAV-LiDAR data

could be used to extract tree height at both individual trees and forest stand levels with a higher accuracy (e.g., Brede et al., 2017; Liu et al., 2018). However, UAV-LiDAR systems may be problematic in estimating individual tree diameter at breast height (DBH) due to attenuation of the laser beam when interacting with dense overstory, and consequently the estimation accuracy will more depend on the stem diameter (Wieser et al., 2017). Given the fact that a Backpack-LiDAR system working in a “down-to-top” view can provide an accurate estimation of DBH and tree location through an individual tree segmentation, it may be used as a complement in forest inventory applications (Polewski et al., 2019). Therefore, a combination of understory with overstory information at a single tree level may solve the problem of under-estimation or over-estimation of the broadleaved forest biomass caused by the low ITS accuracy. Thus, in this study, firstly, a new method was proposed to extract the tree trunk location from Backpack-LiDAR as seed points to assist tree segmentation from UAV-LiDAR data. Secondly, LiDAR variables being important to AGB estimation of *Robinia pseudoacacia* forest at different health levels were identified. Finally, the performance of multiple linear regression (MLR) and random forest (RF) models in estimating forest AGB were evaluated. In addition, the modeling results were analyzed and compared, and relevant issues were discussed as well.

2. Study area and data sets

2.1. Study area

The YRD is situated in the estuary of the Yellow River in Dongying City, Shandong Province, China (Fig. 1a). It has a warm temperate, continental monsoon climate with an annual mean temperature from 11.7–12.6 °C and annual mean precipitation from 530 to 630 mm. The soil salinity has a negative effect on trees growing properly (Zhang, 2013). *Robinia pseudoacacia* is the main tree species suitable for afforestation and has been widely planted in this study area since the 1970s and formed the largest artificial forest in China (Wang et al., 2018). There are four forest areas in the YRD (Fig. 1b) with a total 27.94 km² (Wang et al., 2015a). In this study, Gudao forest was selected as our research area (Fig. 1c).

2.2. Data sets

2.2.1. UAV-LiDAR data

In June 2017, the GreenValley (GreenValley, International, USA, 2019) LiDAR System was implemented to collect LiDAR data. An eight-rotor UAV was used as the platform with a flying height of 120 m above the ground at a speed of 4.8 m·s⁻¹ and a flight radius of 2 km. A Velodyne Puck VLP-16 dual-return laser scanner, an IMU (Novate), and a dual frequency GPS (Novatel) are mounted on the UAV platform. The LiDAR system was configured to emit laser pulses in the near-infrared band with a scanning angle of $\pm 30^\circ$ from nadir; the laser divergence is 0.5 mrad; the spot diameter is about 50 mm, and a laser pulse has a maximum of four echoes with an average point density of 70 m⁻² with a ranging accuracy of 10 mm. The WGS84 coordinate system and UTM projection were adopted. In general, an intensity normalization can improve the estimation accuracy of forest attributes, but this improvement is very minor, so we did not carry out intensity normalization (You et al., 2017). Table 1 shows a summary of laser return density and intensity.

2.2.2. Backpack-LiDAR data

The GreenValley Backpack LiDAR System, consisting of a LiDAR scanner (Velodyne Puck VLP-16), a Position Orientation System (POS) and a handheld touch pad, was applied in this study. In Gudao forest, eight 30 m × 30 m sample plots (Fig. 1) with three health levels (i.e., healthy, medium dieback, severe dieback) (Wang et al., 2015b) were scanned by the Backpack LiDAR System. We designed an “S” shape strip

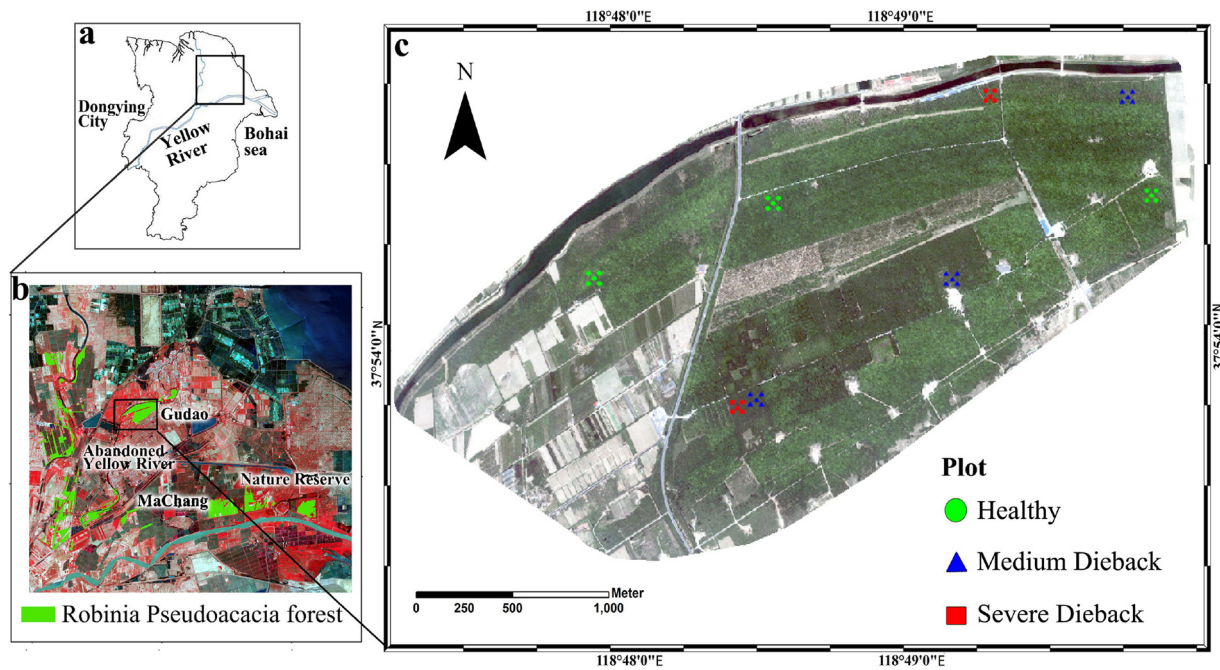


Fig. 1. Study site and the distribution of sample plots. (a) The location of the Yellow River Delta in Dongying City. (b) The distribution of four *Robinia pseudoacacia* forests using Landsat 8 OLI image acquired on June 11, 2013 as a background. (c) The sampling plots located in three different health levels in Gudao forest on an IKONOS image acquired on June 9, 2013 as a background (For interpretation of the references to colour in this figure legend, the reader is referred to the web version of this article).

Table 1

A summary of laser return density and intensity for the study site.

LiDAR returns	Range	Mean	SD
All return height (m)	0-16.5	4.89	4.63
All return density (m ⁻²)	46.2-123.5	70.45	30.2
Last return density (m ⁻²)	0.02-0.8	0.23	0.29
All return intensity	0-255	60.7	74.2

path and placed an artificial marker with known coordinates on the center of a sampling plot (Fig. 2). The laser scanning distance of Backpack LiDAR is 100 m; the scanning frequency is of 300,000 pts·s⁻¹; laser wavelength is 903 nm; the average point density is 7135 m⁻²; the horizontal field of view angle is 360°, and the vertical field of view angle is 15°. The WGS84 coordinate system and UTM projection were also adopted for the data.

2.2.3. Field data

As our previous study (Wang et al., 2015a), in each 30 m × 30 m plot, five 10 m × 10 m subplots were deployed at the four corners and one at the center of each plot. In each subplot, one standard tree was selected. The geographic coordinates of each plot and one standard tree in subplot were recorded by Tianbao GEOXT6000 GPS localizer in June 2017. The tree height and DBH for 40 standard trees were measured using a laser altimeter and a tape measure, respectively.

3. Methods

Fig. 3 shows the overview of the workflow for estimating AGB, mainly divided into two parts: (1) tree segmentation and observed AGB calculation, and (2) UAV-LiDAR based variables extraction and estimation models comparison. We firstly matched and normalized UAV and Backpack LiDAR point clouds. Secondly, the comparative shortest-

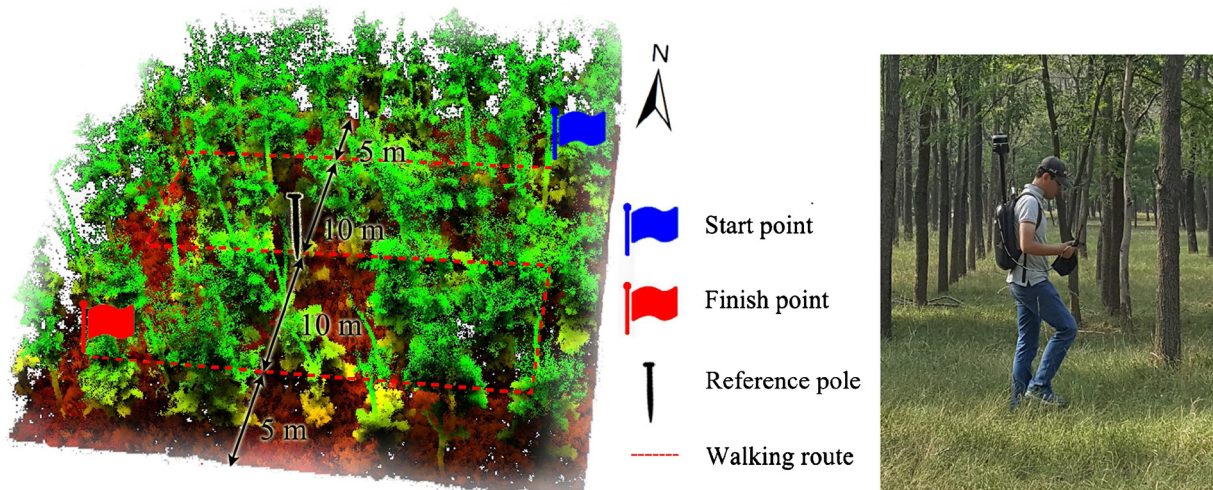


Fig. 2. The trajectory of Backpack-LiDAR point clouds acquisition within one sampling plot (30 m × 30 m).

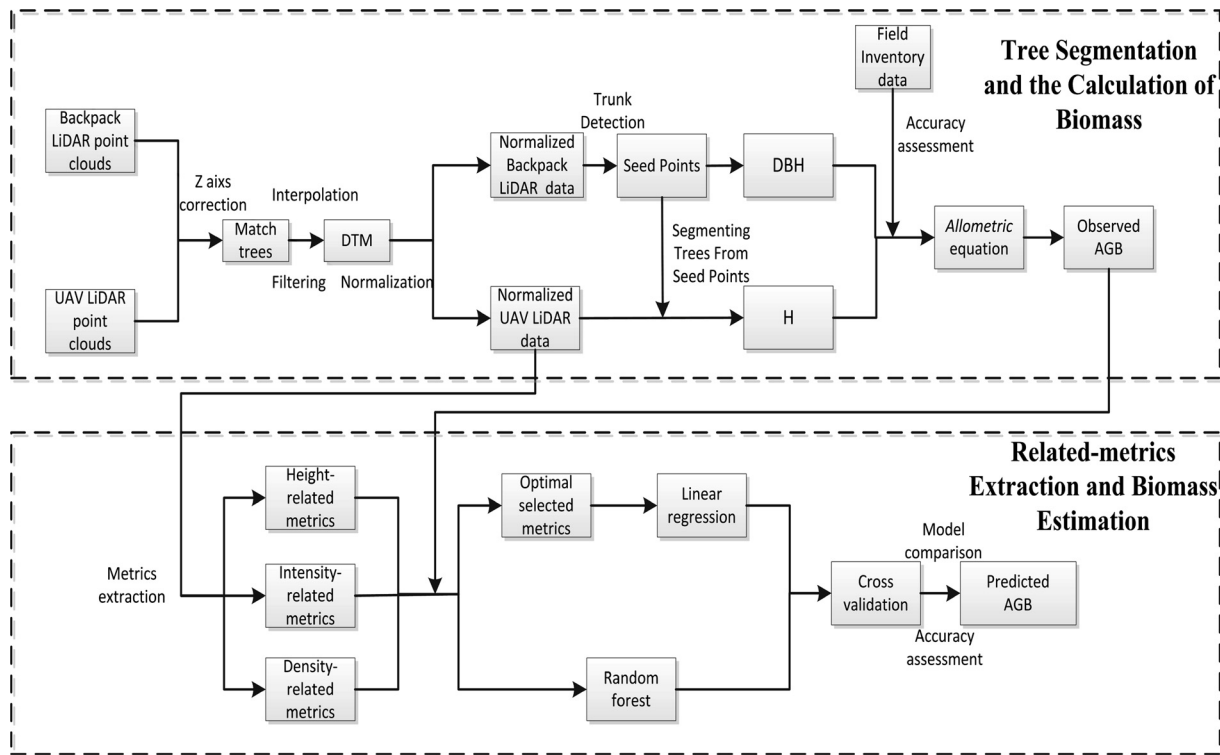


Fig. 3. The overview of the workflow for estimating forest aboveground biomass using LiDAR data.

path algorithm (CSP) (Tao et al., 2015) was used to segment the Backpack-LiDAR point clouds to obtain seed points and single-tree DBH. Using these seed points, individual trees were detected and tree height was obtained from UAV-LiDAR point clouds, and then the observed AGB at eight plots were calculated and accumulated. In the second part, after LiDAR metrics were extracted, the forest AGB predicted results by MLR and RF models were compared. More details about this approach are given below.

3.1. Matching between Backpack-LiDAR and UAV-LiDAR

Since the derived Backpack-LiDAR point clouds were susceptibility to scale variance and planimetric or vertical deviations (Fig. 4(a)), we firstly generated a digital terrain model (DTM) by using an improved progressive triangulated irregular network densification filtering algorithm (Zhao et al., 2016), and then we interpolated the remaining ground points by using the Inverse Distance Weighted algorithm. The point cloud height was normalized by subtracting the ground surface height. After normalization, the ground points of Backpack-LiDAR and UAV-LiDAR data were located in the same plane (Fig. 4(b)). Then we used a method suggested by Polewski et al. (2019) to perform two data matching. At least three pairs of homonymous points were manually selected within the range of the Backpack-LiDAR (Fig. 4(c)) and UAV-LiDAR (Fig. 4(d)), respectively. Finally, the data after matching were normalized again to eliminate the impact caused by z-value difference in point clouds matching. Table 2 shows the registration accuracy of the two types of point clouds data.

3.2. Tree segmentation of LiDAR data

3.2.1. Tree segmentation of Backpack-LiDAR

We applied the GreenValley LiDAR360 commercial software (LiDAR360, 2018) to preprocess the UAV and Backpack acquired data. The algorithm of Density-based spatial clustering of applications with noise (Wu et al., 2013) was used to segment individual tree trunks. A slice with vertical length of 10 cm at 1.3 m height was extracted and

used as input for the CSP algorithm (Tao et al., 2015) and the DBH was then calculated (Fig. 5). After removing the noise data, such as field crew, fallen woods and the reference pole in the LiDAR point clouds, the final seed point files containing the X, Y coordinates and DBH values for each tree were acquired and were used to segment individual trees from the UAV-LiDAR point clouds.

3.2.2. Tree segmentation of UAV-LiDAR

After denoised, the UAV-LiDAR point clouds were normalized again using the same method in section 3.1. A point cloud segmentation (PCS) method (Li et al., 2012) was applied to segment tree crowns. However, in this study, instead of taking the local maximum point of the canopy as the tree apex (seed point) for canopy extraction, the X and Y coordinates of a tree trunk extracted by Backpack-LiDAR were regarded as the seed point. Due to the high data quality of the Backpack-LiDAR, we set the matched and normalized Backpack-LiDAR data as a reference for the accuracy assessment of tree segmentation. Three statistical parameters (Goutte and Gaussier, 2005), which are the detection rate of trees, r (“recall”), the detection accuracy of detected trees, p (“precision”) and the overall accuracy, F (F-score), were used to evaluate the performance of ITS algorithm. The three parameters were defined as follows:

$$r = \frac{TP}{TP + FN}$$

$$p = \frac{TP}{TP + FP} \tag{2}$$

$$F = 2 \times \frac{r \times p}{r + p} \tag{3}$$

where, TP is the number of detected trees in a plot; FN is the number of trees omitted by individual tree segmentation and FP is the number of trees falsely detected in the plot. Meanwhile, the DBH and height values for each standard tree at the subplot extracted by Backpack-LiDAR and UAV-LiDAR, respectively, were evaluated with their corresponding field measurements.

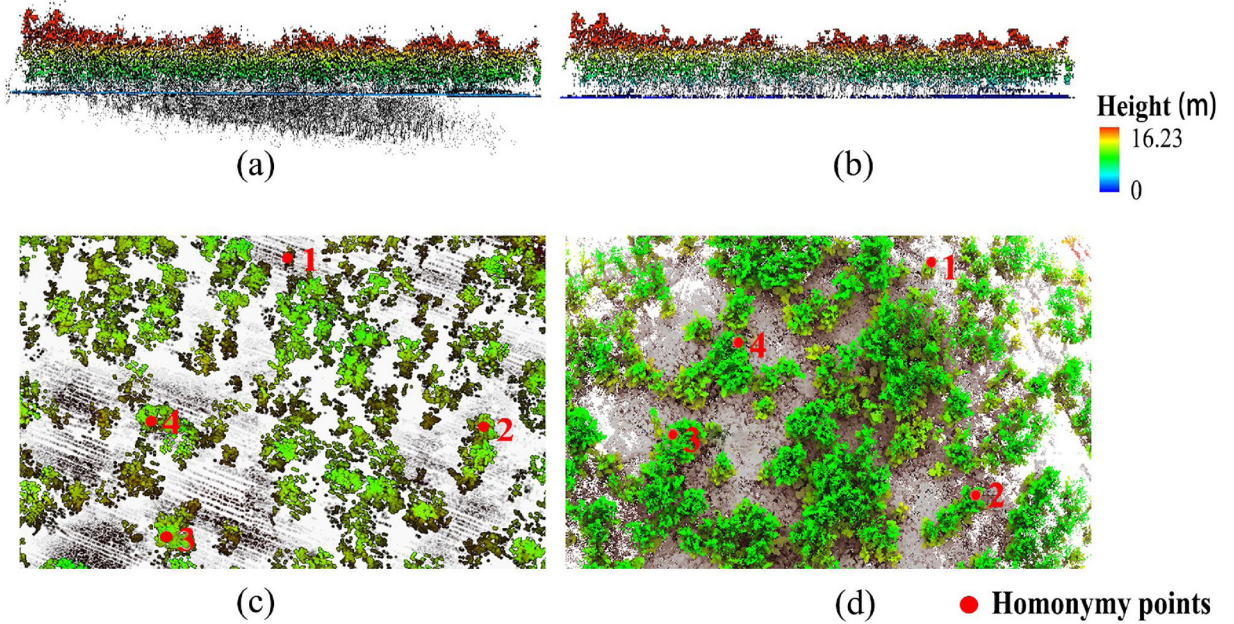


Fig. 4. Backpack-LiDAR and UAV-LiDAR matching schematic diagram. (a) Overlay maps of original Backpack-LiDAR (black) and UAV-LiDAR (chromatic) point clouds, (b) Overlay maps of normalized Backpack-LiDAR and UAV-LiDAR point clouds, (c) and (d) marking numbers for the same tree point cloud in the UAV-LiDAR and Backpack-LiDAR point clouds, respectively.

Table 2
Registration accuracy at eight plots (H: healthy plot, M: medium dieback plot, S: severe dieback plot).

Plot ID	Minimum Error (m)	Maximum Error (m)	Root Mean Square (m)
M1	0.1293	0.4527	0.3253
S2	0.0757	0.6596	0.4125
M3	0.1174	0.5330	0.3855
S4	0.4093	0.6963	0.5392
H5	0.2285	0.3445	0.2688
H6	0.2050	0.1099	0.2806
H7	0.2293	0.4527	0.3620
M8	0.3868	0.5295	0.4319

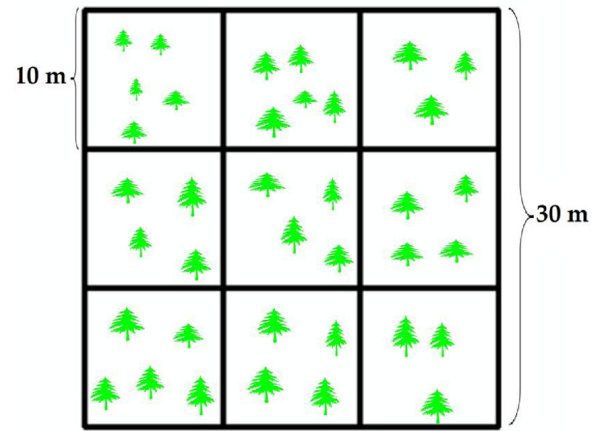


Fig. 6. The schematic diagram for one plot segmentation.

3.3. Biomass calculation of *Robinia pseudoacacia*

The LiDAR data corresponding to the 8 sample plots of 30 m × 30 m with different health levels were cut, and each plot was cut into 9 subplots of 10 m × 10 m, with a total of 72 subplots (Fig. 6). At each subplot, the tree height and DBH extracted by the UAV-LiDAR and Backpack-LiDAR were counted, and the allometric equation of *Robinia pseudoacacia* forest published by the state forestry administration of China (see formulas (4 – 6)) was used to calculate the biomass of trunk (W_s), branch (W_B) and leaf (W_L), and then forest AGB for all subplots was summarized in Table 3.

$$W_s = 0.05527 \times (D^2H)^{0.8576} \tag{4}$$

$$W_B = 0.02425 \times (D^2H)^{0.7908} \tag{5}$$

$$W_L = 0.0545 \times (D^2H)^{0.4574} \tag{6}$$

where D is the DBH (cm) and H is the tree height (m).

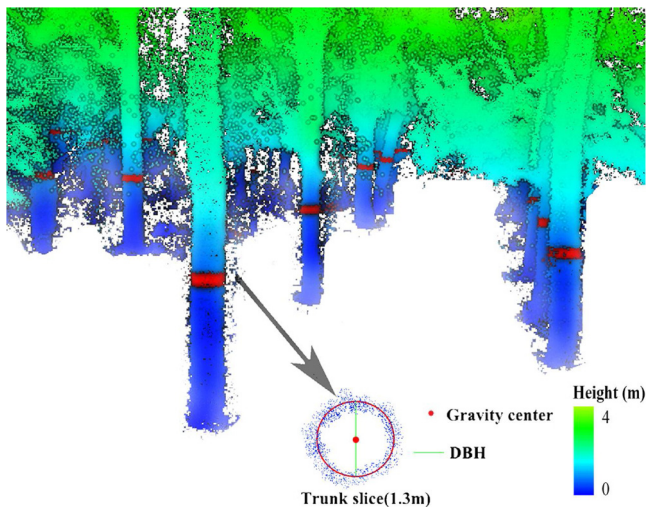


Fig. 5. The demonstrated result of a trunk slice at 1.3 m and the calculated DBH.

Table 3
A summary of field-estimated forest characteristics in 72 subplots with three different health levels.

Variables	Healthy (n = 27)			Medium Dieback (n = 27)			Severe Dieback (n = 18)		
	Range	Mean	SD	Range	Mean	SD	Range	Mean	SD
H (m)	3.45-14.26	9.11	1.69	4.4-16.3	10.5	2.58	4.9-15.4	10.9	2.49
DBH (cm)	5.2-33.4	13.26	4.37	5.2-34.5	16.84	5.42	6.7-29.9	16.6	4.46
AGB (Mg/ha)	15.1-73.42	44.35	13.91	10.46-90.8	43.77	21.09	44.09-104.8	71.77	15.85

Table 4
The summary of LiDAR metrics.

LiDAR metrics	Metrics	Description
Height-related metrics	Percentile height ($H_1, H_5, H_{10}, H_{20}, H_{25}, H_{30}, H_{40}, H_{50}, H_{60}, H_{70}, H_{75}, H_{80}, H_{90}, H_{95}, H_{99}$)	The percentiles of the height distributions (1th, 5th, 10th, 20th, 25th, 30th, 40th, 50th, 60th, 70th, 75th, 80th, 90th, 95th, 99th) of all points above 2 m
	MADmedian (H_{MAD})	Median absolute deviation from the median
	Median of heights (H_{median})	The median of the heights above 2 m of all points
	Mean height (H_{mean})	The mean height above 2 m of all points
	The coefficient of variation of height (H_{cv})	The coefficient of variation of heights of all points above 2 m
	Kurtosis of heights ($H_{kurtosis}$)	The kurtosis of the heights of all points above 2 m
	Interquartile distance of height (H_{IQ})	The Interquartile distance of height of all points above 2 m
	Variance of heights ($H_{variance}$)	The variance of the heights of all points above 2 m
	Absolute average deviation (H_{AAD})	The absolute average deviation of the heights of all points above 2 m
	Standard deviation (H_{std})	The standard deviation of heights of all points above 2 m
	Maximum heights (H_{max})	The maximum height of all points above 2 m
	Skewness of heights (H_{ske})	The skewness of the heights of all points above 2 m
	Density-related metrics	Canopy return density ($D_1, D_2, D_3, D_4, D_5, D_6, D_7, D_8, D_9$)
Canopy cover above 2 m (CC)		Percentages of first returns above 2 m
Intensity-related metrics	Intensity percentile ($I_1, I_5, I_{10}, I_{20}, I_{25}, I_{30}, I_{40}, I_{50}, I_{60}, I_{70}, I_{75}, I_{80}, I_{90}, I_{95}, I_{99}$)	The percentiles of the cumulative intensities distributions (1th, 5th, 10th, 20th, 30th, 40th, 50th, 60th, 70th, 80th, 90th, 95th, 99th) of all points above 2 m
	Laser penetration rate LP	Percentages of last returns above ground
Leaf area index	LAI	LAI is calculated based on equations (7) (8) and (9)

3.4. UAV-LiDAR metrics

Per referring to previous studies (Lim et al., 2003; Næsset, 2002; Næsset and Gobakken, 2008; Ioki et al., 2014; Thomas et al., 2006), metrics extracted from normalized UAV-LiDAR point clouds data in this study include height-related metrics, density-related metrics, intensity-related metrics extracted from all echoes, and LP extracted from the last echo (Table 4). The height-related metrics describe the height percentiles associated with the point clouds height ($H_1, H_5, H_{25}, H_{50}, H_{75}, H_{95}, H_{99}$), such as the height mean (H_{mean}), the height coefficient of variation (H_{cv}), and the height variance ($H_{variance}$), etc. The density-related metrics describe the proportion of the canopy return density, which is the ratio of the number of point clouds above the percentile to the total number of points. The intensity-related metrics are similar to the height-related metrics, and the height value of the point is replaced with the intensity value of the point for calculation. As a basic parameter to characterize vegetation canopy structure, leaf area index (LAI) is defined as half of the surface area of all leaves per a unit surface area (Chen and Black, 1991). Since the dieback for *Robinia pseudoacacia* trees starts from the top crown, the LAI for healthy and dieback forest is different. The LAI metric is derived based on beer-lambert law (Richardson et al., 2009):

$$LAI = -\frac{\cos(ang) \times \ln(GF)}{k} \tag{7}$$

$$ang = \frac{\sum_{i=1}^n angle_i}{n} \tag{8}$$

$$GF = \frac{n_{ground}}{n} \tag{9}$$

where ang is the average scan angle; GF is the gap fraction; k is the extinction coefficient. In this study, we assumed that the distribution of leaf angle is spherical and $k = 0.5$ (Richardson et al., 2009). $angle_i$ is the

scan angle of the i th LiDAR point which is recorded in the UAV las file; n_{ground} is the number of ground points and n is the number of LiDAR points. A total of 53 metrics (Table 4) extracted from UAV-LiDAR by using LiDAR360 software were prepared for AGB prediction in the Gudao forest by MLR and RF models.

3.5. Model development

Different modeling methods have different effects on the quality of results (Straub et al., 2010). In this study, the parametric and non-parametric methods were compared. Both MLR and RF regression models were used to estimate the forest AGB for each subplot and run with the measured forest AGB and the LiDAR data derived metrics as the dependent and independent variables, respectively. MLR is a very simple parametric method that has the ability to deal with dependencies on or correlations with the predictors and it has been frequently used in AGB estimation (e.g., Fassnacht et al., 2014; Morin et al., 2019). Previous studies have used a logarithmic transformation of dependent and independent variables to improve the fitting ability of the model (Næsset et al., 2005). Because there were negative numbers in our LiDAR metrics, the logarithmic transformation is not carried out in order to avoid information loss. Before adopting the MLR model, WEKA software (Hall et al., 2009) was used to select optimal LiDAR derived metrics. The CfsSubsetEval evaluator in WEKA evaluates the predictive ability of each attribute (i.e., metric in this study) and its mutual redundancy and tends to select attributes that are highly correlated with the target attribute (i.e. dependent variable in this study) but less correlated with each other (Hall, 1998). We employed a forward search from the empty attribute set to filter the attribute subset. After selecting the optimal candidate metrics, MLR was performed to obtain the optimal AGB model. A leave-one-out cross-validation (LOOCV) method (Bengio and Grandvalet, 2004) that each of these samples is estimated using all the other samples was used for assessing

the performance of the calibrated MLR model.

RF is a decision-tree based, distribution-free (non-parametric) classification algorithm that can avoid the over-fitting problem and it is robust to outliers and noise (Breiman, 2001). For RF, two parameters, *ntree* and *mtry*, need to be set. The *ntree* represents the total number of trees running in the regression model, and *mtry* represents the number of variables that can be split on each node of the tree (Mutanga et al., 2012; Yu et al., 2011). In this study, in order to obtain better *ntree* and *mtry* for predicting forest AGB at different health levels, we optimized the two parameters based on the error distribution and interpretation rate, and the *ntree* value of 1000 and *mtry* value of one third of predictive variables were acquired. The relative importance of each metric was ranked by calculating an increase in the mean squared error of the model after removing this variable. The accuracy assessment was carried out also by using the LOOCV method.

The accuracy of the regression models was evaluated by determination coefficient (R^2), root mean square error (RMSE) and relative root mean square error (rRMSE) expressed as follows:

$$R^2 = 1 - \frac{\sum_{i=1}^n (x_i - \hat{x}_i)^2}{\sum_{i=1}^n (x_i - \bar{x}_i)^2} \tag{10}$$

$$RMSE = \sqrt{\frac{1}{n} \sum_{i=1}^n (x_i - \hat{x}_i)^2} \tag{11}$$

$$rRMSE = \frac{RMSE}{\bar{x}} \times 100\% \tag{12}$$

where x_i is the measured value for plot i ; \hat{x}_i is the estimated value for plot i ; \bar{x}_i is the observed mean value for subplot i ; \bar{x} is the observed mean value for all plots; n is the number of subplots.

4. Results

4.1. Individual tree segmentation

At the eight *Robinia pseudoacacia* forests plots, the ITS method based on the Backpack-LiDAR achieved a high accuracy (Table 5). The r value ranged from 0.95 to 1 with a mean value of 0.97; the p value was between 0.79 and 0.91 with a mean value of 0.87; and the F value was between 0.87 and 0.94 with a mean value of 0.92.

The UAV-LiDAR tree segmentation method using seed points derived from Backpack-LiDAR also achieved a higher accuracy (Table 6). The r value ranged between 0.97 and 1, and the mean value was 0.98; the p value was 1; the F value ranged between 0.98 and 1, and the mean value was 0.99.

4.2. Evaluation of DBH and H extracted from LiDAR

Fig. 7(a) shows the comparison between the measured DBHs of

Table 5

Accuracy assessment for the ITS method based on Backpack-LiDAR data at the eight sample plots (H: healthy plot, M: medium dieback plot, S: severe dieback plot).

Plot ID	Number of trees	Number of Segmented trees	TP	FP	FN	r	p	F
M1	59	72	57	15	2	0.97	0.79	0.87
S2	80	84	77	7	3	0.96	0.91	0.94
M3	59	70	59	11	0	1	0.84	0.91
S4	125	136	119	17	6	0.95	0.85	0.91
H5	114	133	114	19	0	1	0.86	0.92
H6	105	107	100	7	5	0.95	0.93	0.94
H7	52	61	52	9	0	1	0.85	0.92
M8	63	73	62	11	1	0.98	0.85	0.91
Mean	657	736	640	96	17	0.97	0.87	0.92

Table 6

Accuracy assessment for the ITS method based on UAV-LiDAR tree segmentation in the eight sample plots (H: healthy plot, M: medium dieback plot, S: severe dieback plot).

Plot ID	Number of trees	Number of Segmented trees	TP	FP	FN	r	p	F
M1	59	58	58	0	1	0.98	1	0.99
S2	80	80	80	0	0	1	1	1
M3	59	58	0	0	1	0.98	1	0.99
S4	125	122	122	0	3	0.98	1	0.99
H5	114	113	113	0	1	0.99	1	0.99
H6	105	105	105	0	0	1	1	1
H7	52	51	51	0	1	0.98	1	0.99
M8	63	61	61	0	2	0.97	1	0.98
Mean	657	648	590	0	9	0.98	1	0.99

standard trees in 40 subplots and the mean value of the DBH extracted from Backpack-LiDAR in these subplots ($R^2 = 0.94$, $RMSE = 1.02$ cm). Fig. 7(b) shows the comparison between the measured heights of standard trees in 40 subplots and the mean value of the tree height extracted from UAV-LiDAR in these subplots based on seed points ($R^2 = 0.83$, $RMSE = 1.48$ m). By comparing the measured values with the tree DBH and height extracted from the LiDAR data, the credibility of the abstracted DBH and height can be proved.

4.3. MLR method for biomass estimation

Table 7 presents the forest AGB estimation results by MLR models and the LiDAR derived metrics selected by WEKA. The three MLR models produced a moderate estimation accuracy with best R^2 and RMSE values at the medium dieback forest plots. In addition to the selection of height-related metrics and density-related metrics, LP was selected at both healthy and medium dieback plots, and LAI was selected in severe dieback plots. Fig. 8 shows the cross-validation results of the predicted AGB by the MLR models and field-estimated AGB in the three health-level *Robinia pseudoacacia* forest.

4.4. RF method for biomass estimation

Fig. 9 shows the cross-validation results of field-estimated AGB and the predicted AGB by RF models. Overall, the fitted models based on the RF outperformed those on the MLR. The importance ranks of the LiDAR derived metrics determined by the RF models (Fig. 10) indicate that *CC* and *LP* are the most important LiDAR metrics in the AGB estimation model in the healthy forests. In the medium dieback forests, the most important LiDAR metric also is *CC*, followed by H_{60} and H_{75} . In the severe dieback forests, the most important LiDAR metric is H_{99} , followed by D_2 .

5. Discussion

5.1. The comparison of segmentation accuracy

At each plot, we used the CSP algorithm (Tao et al., 2015) to segment individual trees with Backpack-LiDAR data (overall accuracy of 0.92) and obtained the DBH for an individual tree with a higher accuracy ($R^2 = 0.94$, $RMSE = 1.02$ cm for one standard tree in each subplot). Because of the high density of the Backpack-LiDAR point clouds, the non-tree point clouds such as the fallen trees, reference poles and persons (Fig. 11) could be manually removed. If we did not use the tree location derived from the Backpack-LiDAR as seed points, the overall accuracy for ITS method would drop 0.17 (from 0.99 to 0.82, see a comparison of Table 6 with Table 8) with over- or under-segmentation for majority trees. This is because we used PCS algorithm (Li et al., 2012) to extract individual tree treetops and crowns. The PCS algorithm used top-to-bottom region growing method to determine the

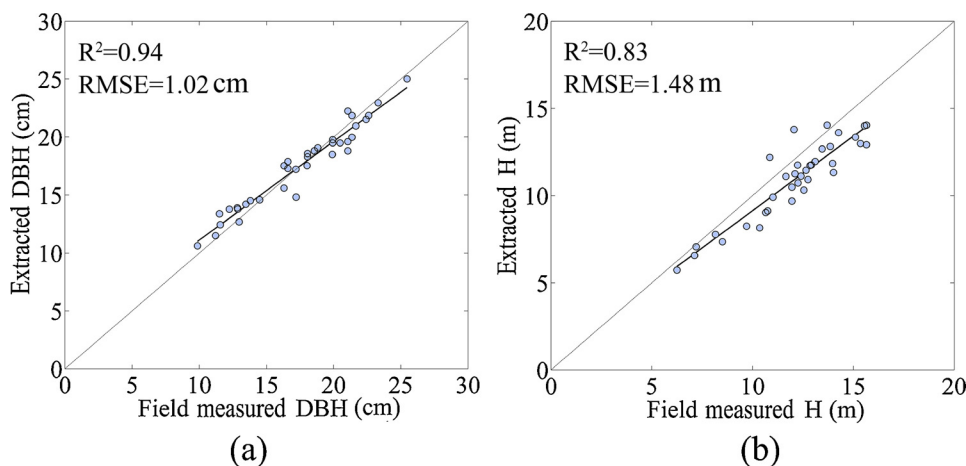


Fig. 7. Comparisons between field measured DBH and H and extracted DBH from Backpack-LiDAR and H from UAV-LiDAR data. (a) For DBH, and (b) for H.

Table 7

The summary of linear predictive models and accuracy assessment results at the three different health plots.

Plot	Predictive Models	R ²	RMSE (Mg/ha)	rRMSE (%)
Healthy	$W_{AGB} = 833.05 \times LP + 148.16 \times D_9 + 0.1617 \times I_{80} - 20.81$	0.72	7.5	16.6
Medium Dieback	$W_{AGB} = 369.56 \times LP - 217.48 \times D_4 + 0.37 \times I_{60} - 17.49$	0.77	10.05	22.9
Severe Dieback	$W_{AGB} = 12.98 \times LAI + 6.07 \times H_{20} - 5.54 \times H_{90} + 16.20 \times H_{99} + 103.01 \times D_2 + 130.15 \times D_4 - 159.81$	0.70	8.67	12.1

spacing between trees and is successful in coniferous forests; however, in broadleaved forests, it is difficult to detect tree tops from the densely intertwined forest canopies in healthy and medium dieback forests (Fig. 12), leading to a low segmentation accuracy (Table 8). Therefore, in this study, we combined Backpack-LiDAR and UAV-LiDAR data. Each tree trunk’s coordinates extracted by the ITS method from the Backpack-LiDAR was used as seed points for UAV-LiDAR segmentation, leading to an improvement of the overall accuracy of individual tree detection. Fig. 13 shows the segmentation results of Backpack-LiDAR and UAV-LiDAR, respectively. On the other hand, if the individual trees would not be segmented correctly, we could not obtain the individual tree height from UAV-LiDAR data, and thus the both individual tree- and plot-level field-estimated AGB could not be calculated.

5.2. The comparison between MLR and RF models

In this study, the allometric equation of forest AGB (Eqs. (4 – 6)) required two parameters: tree height and DBH, which are usually obtained by measuring the individual tree height and DBH at sample plots. This method is accurate but time-consuming. It has been proved

that the airborne/UAV LiDAR point clouds can be used to extract tree height information (Næsset and Bjerknes, 2001; Yu et al., 2011) and terrestrial/backpack LiDAR data can be used to extract DBH (Lovell et al., 2011; Maas et al., 2008) with a high accuracy. Our study result also confirmed this point (Fig. 7). Therefore, we adopted tree DBH and height derived from the Backpack-LiDAR and UAV-LiDAR, respectively, to calculate field-estimated AGB.

Although the use of tree height derived from UAV-LiDAR and DBH derived from Backpack-LiDAR has its benefits, the time required by hardware calculation and data processing will be long. Hence, we only applied this method to 72 subplots (10 m × 10 m) to calculate field-estimated forest AGB based on an allometric equation (Eqs. (4 – 6)). And then the 53 metrics (Table 4) extracted from UAV-LiDAR data were regressed with above field-estimated forest AGB from the same subplots. Using this method, we could predict the AGB of *Robinia pseudoacacia* forest over the whole study area.

In this study, two different modeling methods were used to estimate the forest AGB, the MLR and RF models. The modeling results indicate that RF performed better than that of MLR (R² of 0.91-0.95 vs. R² of 0.70-0.77, rRMSE of 6.5 %–10.6 % vs. rRMSE of 12.1 %–22.9 %). In the

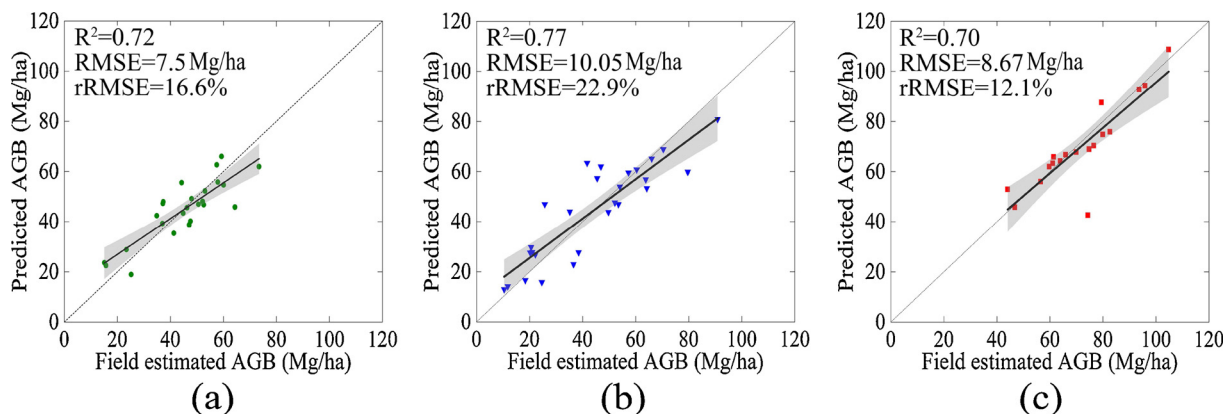


Fig. 8. Field-estimated forest AGB (Mg/ha) versus predicted forest AGB (Mg/ha) using MLR models at the (a) healthy subplots, (b) medium dieback subplots, and (c) severe dieback subplots. The solid lines were the fitting models; the gray areas showed 95 % confidence intervals of the fitting models.

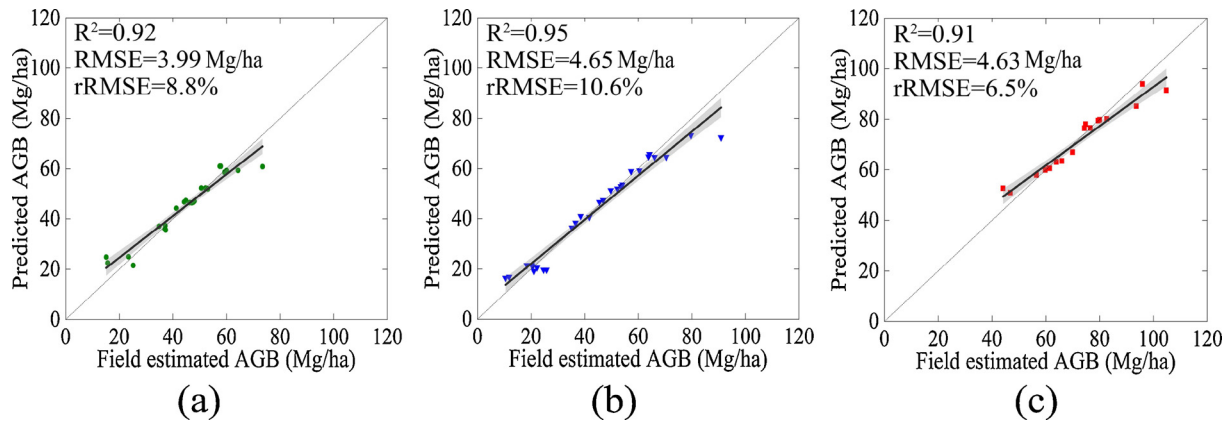


Fig. 9. Field-estimated forest AGB (Mg/ha) versus predicted forest AGB (Mg/ha) using RF models at the (a) healthy subplots, (b) medium dieback subplots, and (c) severe dieback subplots. The solid lines were the fitting models; the gray areas were 95 % confidence intervals of the fitting models.

MLR models, LP (the percentage of the last echo above the ground in all point clouds) was screened out by WEKA for both healthy and medium dieback forests, but not for severe dieback forests. This is due to canopy closure in healthy and medium dieback forests, which prevents the first laser echo from penetrating the canopy completely, while the last laser echo penetrating the upper canopy can provide the lower canopy information. However, due to the top crown dieback in the severe dieback forest, most of the first laser echoes can penetrate into the forest canopy layer, while the last echo mostly reflects the ground points. When these last echo data reflecting the ground points were removed, LP cannot reflect the canopy vertical variation in severe dieback forest. According to the importance ranking of variables by random forest model, the top ten variables in healthy forest and medium dieback forest included variables relating to canopy horizontal distribution, height related and intensity related distribution. LP was selected again by RF model in healthy forests, and the correlation coefficient between LP and AGB is 0.77, indicating that LP played an important role in the forest AGB prediction in the broadleaved forest with a highly intertwined canopy (Ioki et al., 2014).

Given the eight 30 m × 30 m plots, we had to divide each 30 m × 30 m plot into nine 10 m × 10 m subplots. However, since the size of

the subplot was relatively small, the tree crowns in other plots always cross a boundary, which increases the edge effect. Frazer et al. (2011) confirmed that with the increasing size of the plot, the accuracy of the AGB model will increase to a certain threshold and then stabilizes. Increasing a number of sample plots is our future work.

5.3. Impact of forest health conditions on biomass estimation

Robinia pseudoacacia forest in the study area suffered from different degrees of dieback. However, allometric equations (Eqs. (4 – 6)) for AGB estimation do not include parameters distinguishing the different forest health conditions. In order to find whether the forest health status may have any influences on the forest AGB estimation, we did a statistical analysis on the measured data of tree height and DBH collected from different health-level *Robinia pseudoacacia* forest in 2013, 2014 and 2017 in the study area. The investigated plot was 30 m × 30 m, in which 5 subplots of 10 m × 10 m were selected, and a standard tree was selected from each subplot to measure its DBH and height. A total of 185 healthy trees, 100 medium dieback trees and 50 severe dieback trees were selected. Relevant statistics were performed on measured tree heights and DBHs of 335 trees, and the 95 % of the

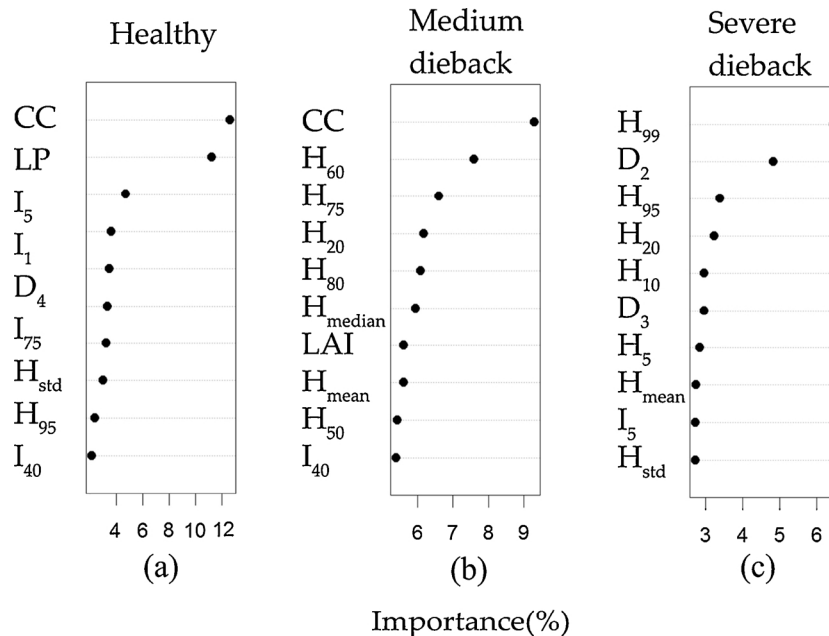


Fig. 10. Random Forest ranked LiDAR derived metrics based on their regression importance values at different health-level forest plots: (a) healthy, (b) medium dieback, and (c) severe dieback.

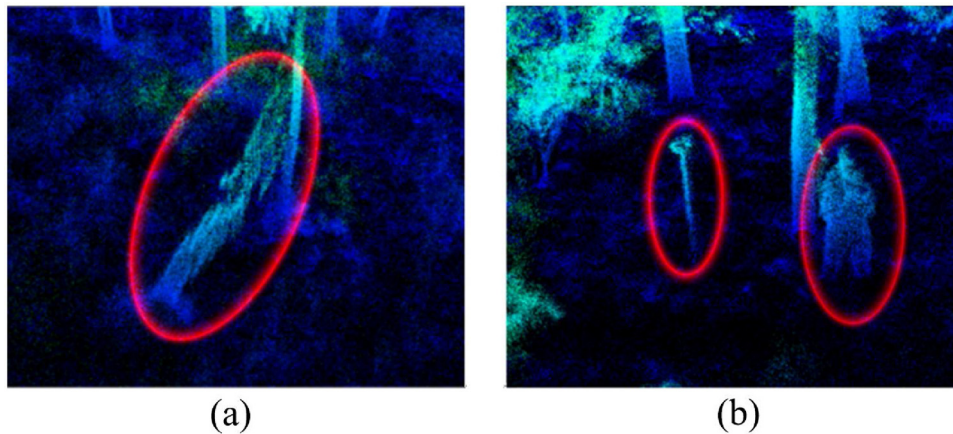


Fig. 11. The noises in the Backpack-LiDAR point cloud data. (a) A fallen wood, and (b) a reference pole and a person.

Table 8

Accuracy assessment for UAV-LiDAR tree segmentation without seed points derived from the Backpack-LiDAR data at the eight different health-level plots (H: healthy, M: medium dieback, S: severe dieback).

Plot ID	Number of trees	Number of Segmented trees	TP	FP	FN	r	p	F
M1	59	36	36	0	23	0.61	1	0.76
S2	80	84	74	10	6	0.92	0.88	0.89
M3	59	64	50	14	9	0.85	0.78	0.81
S4	125	126	117	9	8	0.93	0.92	0.92
H5	114	65	65	0	49	0.57	1	0.73
H6	105	67	67	0	38	0.63	1	0.77
H7	52	48	42	6	10	0.81	0.87	0.83
M8	63	36	36	0	27	0.57	1	0.73
Mean	657	526	487	39	170	0.74	0.92	0.82

confidence interval was calculated. The results demonstrated that the fitting curves of DBH and height for the different health conditions were very similar, and the 95 % confidence areas overlapped without a statistically significant difference (Fig. 14). Therefore, we did not distinguish the different health conditions of *Robinia pseudoacacia* forests when using the allometric equation. The tree AGB calculation includes three parts in the allometric equations: trunk, branches and leaves. For the dieback forest, there will be an overestimation of leaf biomass, which provides us a basis of modifying the existing allometric equation in the future study (Shao et al., 2018).

We also found that the largest mean AGB values appeared at the severe dieback forest subplots, while healthy and medium dieback forest shared almost the same biomass accumulations (Table 3). Hence,

the health levels of *Robinia pseudoacacia* forest have no relationship with the field-estimated AGB. This is because forest health levels in the study area, which include healthy, medium dieback, severe dieback or death, were evaluated on a range of values in the CCCG (the United States Forest Service Crown Condition Classification Guide) standard (Wang et al., 2015a). The CCCG indicators (Schomaker et al., 2007), including live crown ratio, crown density, crown diameter, dieback, and foliar transparency, mostly reflected crown vigour at a single tree level. Our previous study showed that near infrared reflectance band and texture features derived from the high spatial resolution satellite image, such as IKONOS, could efficiently differentiate three health levels of *Robinia pseudoacacia* forest (Wang et al., 2015b). To determine the forest AGB, the three dimensional structures of forests, such as tree height and DBH, may not be necessarily associated with the single tree crown vigour status. During the field investigation, we also found that some trees at the healthy and medium dieback forest plots grew short and small with smaller tree height and DBH values, while at the severe dieback forest plots, most trees were withered or dead, and only one or two trees had grown tall and large, leading to a higher AGB value (Table 3). This is because the growth of *Robinia pseudoacacia* trees in Gudao was suppressed by high soil moisture due to lower elevation or near a river or road (Wang et al., 2016).

From our communications with a local forest manager, we know that the *Robinia pseudoacacia* trees in the Gudao forest were planted in the mid-1980s, and dieback or dead trees were rarely cut down and replanted. Only the trees along both sides of the main road across the forest area were well managed and thus in a healthy condition. This changed our previous point of view that the short and small trees at the healthy and medium dieback forest plots were supposed to be recently

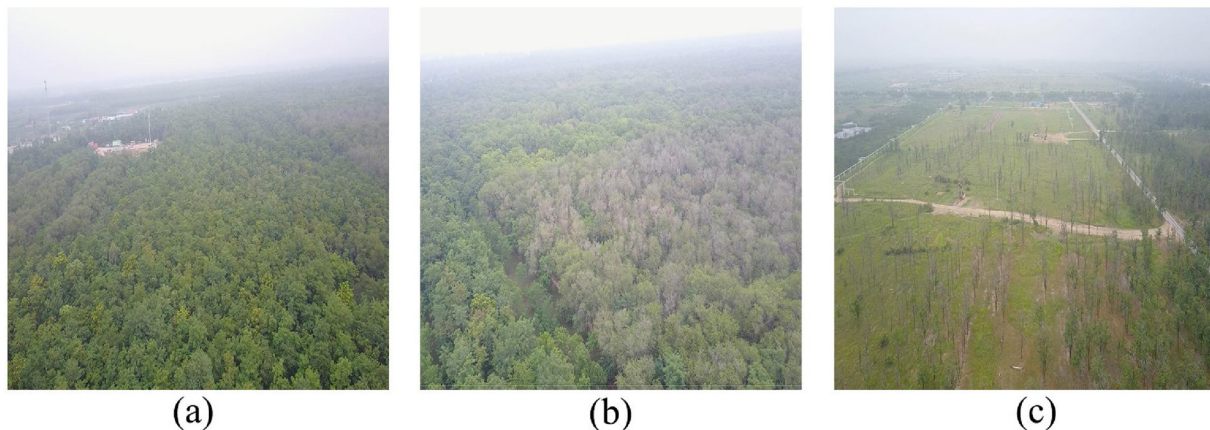


Fig. 12. Pictures taken by UAV in the *Robinia pseudoacacia* forest at different health levels: (a) healthy, (b) medium dieback, and (c) severe dieback.

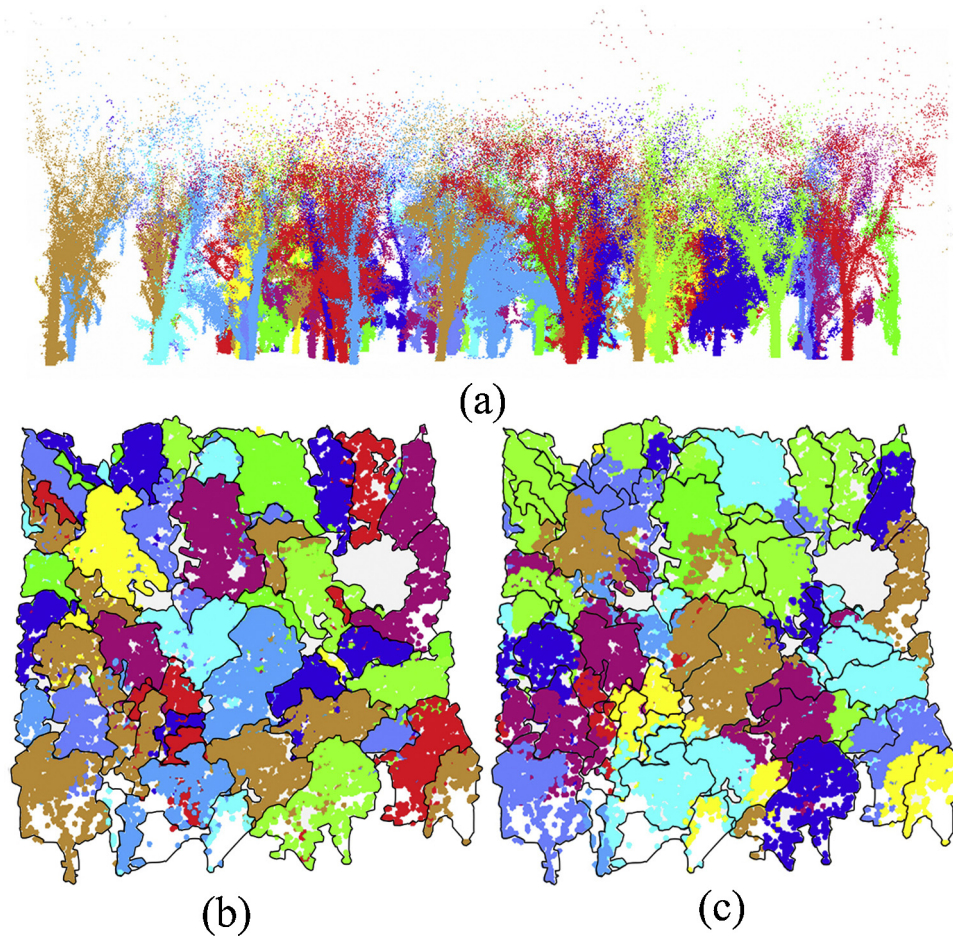


Fig. 13. The schematics of tree segmentation results. (a) The segmentation results of Backpack-LiDAR data, (b) the segmentation results of UAV-LiDAR based on seed points, and (c) the segmentation results of UAV-LiDAR without seed points. Different colors represent different trees. The polygon patches overlaid on (b) and (c) are individual trees or tree crowns derived from visual interpretation.

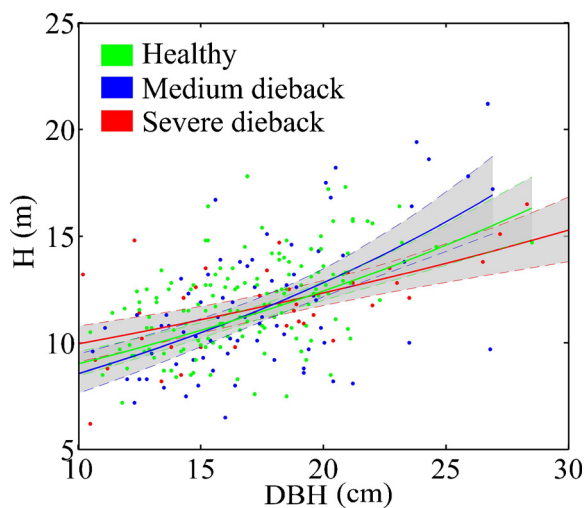


Fig. 14. Relationships between DBH and height (H). The solid lines were the fitting models; the gray areas were 95 % confidence intervals of the fitting models.

replanted after dieback trees were removed, and thus the young age of trees was thought to be a reason for the lower forest AGB (Zheng et al., 2007).

This may provide us a new idea on how to classify the forest health levels. The five crown vigour indicators at a single tree level from CCCG

standard may not be suitable for the health level classification of the *Robinia pseudoacacia* trees, which have been suffered from long term and slow disturbance in our study area. While forest attributes at both single tree and stand levels, such as tree biomass, canopy cover and tree height, are able to be acquired from both field and LiDAR point clouds, they may be more effective for determining the health levels of *Robinia pseudoacacia* forest.

6. Conclusions

In this study, two kinds of point cloud data, UAV-LiDAR and Backpack-LiDAR, were used for individual tree detection and AGB estimation at different health levels of the *Robinia pseudoacacia* forest. Three conclusions were derived from the experimental results as follows:

- (1) The tree trunk positions extracted from the Backpack-LiDAR data could be used as the seed points for individual tree segmentation (ITS) by using UAV-LiDAR data. This method could effectively improve the tree segmentation accuracy of broadleaved forest in the growing season (total accuracy $F = 0.99$). With the development of LiDAR technology, laser detectors and carrying platforms are becoming lighter and more diversified. The combination of UAV with Backpack LiDAR data can effectively solve the problem of under- or over-segmentation using ITS method in broadleaved forests.
- (2) Canopy coverage, LP, and intensity-related metrics reflecting vegetation health status play an important role in AGB estimation of

Robinia pseudoacacia forest.

- (3) RF model resulted in a higher accuracy in predicting forest AGB than MLR model.

Declaration of Competing Interest

The authors declare no conflict of interest.

Acknowledgment

The research was supported by the National Natural Science Foundation of China (No. 41471419 and No. 31971579).

References

- Basuki, T.M., Van Laake, P.E., Skidmore, A.K., Hussin, Y.A., 2009. Allometric equations for estimating the above-ground biomass in tropical lowland Dipterocarp forests. *For. Ecol. Manage.* 257, 1684–1694. <https://doi.org/10.1016/j.foreco.2009.01.027>.
- Bengio, Y., Grandvalet, Y., 2004. No unbiased estimator of the variance of k-fold cross-validation. *J. Mach. Learn. Res.* 5, 1089–1105.
- Brede, B., Lau, A., Bartholomeus, H.M., Kooistire, L., 2017. Comparing RIEGL RiCOPTER UAV LiDAR derived Canopy height and DBH with terrestrial LiDAR. *Sensors* 17, 2371. <https://doi.org/10.3390/s17102371>.
- Breiman, L., 2001. Random forests. *Mach. Learn.* 45, 5–32.
- Cao, L., Coops, N.C., Innes, J.L., Sheppard, S.R., Fu, L., Ruan, H., She, G., 2016. Estimation of forest biomass dynamics in subtropical forests using multi-temporal airborne LiDAR data. *Remote Sens. Environ.* 178, 158–171. <https://doi.org/10.1016/j.rse.2016.03.012>.
- Chen, J.M., Black, T.A., 1991. Measuring leaf area index of plant canopies with branch architecture. *Agric. For. Meteorol.* 57, 1–12. [https://doi.org/10.1016/0168-1923\(91\)90074-z](https://doi.org/10.1016/0168-1923(91)90074-z).
- Dandois, J., Olano, M., Ellis, E., 2015. Optimal altitude, overlap, and weather conditions for computer vision UAV estimates of forest structure. *Remote Sens. (Basel)* 7, 13895–13920. <https://doi.org/10.3390/rs71013895>.
- Fassnacht, F.E., Hartig, F., Latifi, H., Berger, C., Hernández, J., Corvalán, P., Koch, B., 2014. Importance of sample size, data type and prediction method for remote sensing-based estimations of aboveground forest biomass. *Remote Sens. Environ.* 154, 102–114. <https://doi.org/10.1016/j.rse.2014.07.028>.
- Frazer, G.W., Magnussen, S., Wulder, M.A., Niemann, K.O., 2011. Simulated impact of sample plot size and co-registration error on the accuracy and uncertainty of LiDAR-derived estimates of forest stand biomass. *Remote Sens. Environ.* 115, 636–649. <https://doi.org/10.1016/j.rse.2010.10.008>.
- Goutte, C., Gaussier, E., 2005. A probabilistic interpretation of precision, recall and F-score, with implication for evaluation. In: Santiago de Compostela, Spain, 21–23 March. Proceedings of the 27th European Conference on IR Research Vol. 3408. pp. 345–359. https://doi.org/10.1007/978-3-540-31865-1_25.
- GreenValley, International, USA. (2019) <https://greenvalleyintl.com>.
- Hall, M.A., 1998. Correlation-based Feature Subset Selection for Machine Learning. Thesis Submitted in Partial Fulfillment of the Requirements of the Degree of Doctor of Philosophy at the University of Waikato.
- Hall, M., Frank, E., Holmes, G., Pfahringer, B., Reutemann, P., Witten, I.H., 2009. The WEKA data mining software: an update. *ACM SIGKDD Explor. Newsl.* 11, 10–18. <https://doi.org/10.1145/1656274.1656278>.
- Hall, S.A., Burke, I.C., Box, D.O., Kaufmann, M.R., Stoker, J.M., 2005. Estimating stand structure using discrete-return lidar: an example from low density, fire prone ponderosa pine forests. *For. Ecol. Manage.* 208, 189–209. <https://doi.org/10.1016/j.foreco.2004.12.001>.
- Hermosilla, T., Ruiz, L.A., Kazakova, A.N., Coops, N.C., Moskal, L.M., 2014. Estimation of forest structure and canopy fuel parameters from small-footprint full-waveform LiDAR data. *Int. J. Wildl. Fire* 23, 224–233. <https://doi.org/10.1071/wf13086>.
- Hudak, A.T., Strand, E.K., Vierling, L.A., Byrne, J.C., Eitel, J.U., Martinuzzi, S., Falkowski, M.J., 2012. Quantifying aboveground forest carbon pools and fluxes from repeat LiDAR surveys. *Remote Sens. Environ.* 123, 25–40. <https://doi.org/10.1016/j.rse.2012.02.023>.
- Ioki, K., Tsuyuki, S., Hirata, Y., Phua, M.H., Wong, W.V.C., Ling, Z.Y., Saito, H., Takao, G., 2014. Estimating above-ground biomass of tropical rainforest of different degradation levels in Northern Borneo using airborne LiDAR. *For. Ecol. Manage.* 328, 335–341. <https://doi.org/10.1016/j.foreco.2014.06.003>.
- Lefsky, M.A., Cohen, W.B., Parker, G.G., Harding, D.J., 2002. Lidar remote sensing for ecosystem studies. *BioScience* 52, 19–30.
- Li, W., Guo, Q., Jakubowski, M.K., Kelly, M., 2012. A new method for segmenting individual trees from the lidar point cloud. *Photogramm. Eng. Remote Sensing* 78, 75–84. <https://doi.org/10.14358/pers.78.1.75>.
- Lim, K., Treitz, P., Wulder, M., St-Onge, B., Flood, M., 2003. LiDAR remote sensing of forest structure. *Prog. Phys. Geogr.* 27, 88–106. <https://doi.org/10.1191/0309133303pp360ra>.
- Liu, K., Shen, X., Cao, L., Wang, G., Cao, F., 2018. Estimating forest structural attributes using UAV-LiDAR data in Ginkgo plantations. *ISPRS J. Photogramm. Remote Sens.* 146, 465–482. <https://doi.org/10.1016/j.isprsjprs.2018.11.001>.
- Liu, L., Lim, S., Shen, X., Yebra, M., 2019. A hybrid method for segmenting individual trees from airborne lidar data. *Comput. Electron. Agric.* 163 <https://doi.org/10.1016/j.compag.2019.104871>. 104871.
- Lorenzen, B., Jensen, A., 1988. Reflectance of blue, green, red and near infrared radiation from wetland vegetation used in a model discriminating live and dead above ground biomass. *New Phytol.* 108, 345–355. <https://doi.org/10.1111/j.1469-8137.1988.tb04173.x>.
- Lovell, J.L., Jupp, D.L., Culvenor, D.S., Coops, N.C., 2003. Using airborne and ground-based ranging lidar to measure canopy structure in Australian forests. *Can. J. Remote Sens.* 29, 607–622. <https://doi.org/10.5589/m03-026>.
- Lovell, J.L., Jupp, D.L.B., Newnham, G.J., Culvenor, D.S., 2011. Measuring tree stem diameters using intensity profiles from ground-based scanning lidar from a fixed viewpoint. *ISPRS J. Photogramm. Remote Sens.* 66, 46–55. <https://doi.org/10.1016/j.isprsjprs.2010.08.006>.
- Lu, X., Guo, Q., Li, W., Flanagan, J., 2014. A bottom-up approach to segment individual deciduous trees using leaf-off lidar point cloud data. *ISPRS J. Photogramm. Remote Sens.* 94, 1–12. <https://doi.org/10.1016/j.isprsjprs.2014.03.014>.
- Maas, H.G., Bienert, A., Scheller, S., Keane, E., 2008. Automatic forest inventory parameter determination from terrestrial laser scanner data. *Int. J. Remote Sens.* 29, 1579–1593. <https://doi.org/10.1080/01431160701736406>.
- Morin, D., Planells, M., Guyon, D., Villard, L., Mermoz, S., Bouvet, A., Thevenon, H., Dejoux, J.-F., Le Toan, T., Dedieu, G., 2019. Estimation and mapping of forest structure parameters from open access satellite images: development of a generic method with a study case on coniferous plantation. *Remote Sens.* 11, 1275. <https://doi.org/10.3390/rs11111275>.
- Mutanga, O., Adam, E., Cho, M.A., 2012. High density biomass estimation for wetland vegetation using WorldView-2 imagery and random forest regression algorithm. *Int. J. Appl. Earth Obs. Geoinf.* 18, 399–406. <https://doi.org/10.1016/j.jag.2012.03.012>.
- Næsset, E., 2002. Predicting forest stand characteristics with airborne scanning laser using a practical two-stage procedure and field data. *Remote Sens. Environ.* 80, 88–99. [https://doi.org/10.1016/S0034-4257\(01\)00290-5](https://doi.org/10.1016/S0034-4257(01)00290-5).
- Næsset, E., Bjerknes, K.O., 2001. Estimating tree heights and number of stems in young forest stands using airborne laser scanner data. *Remote Sens. Environ.* 78, 328–340. [https://doi.org/10.1016/S0034-4257\(01\)00228-0](https://doi.org/10.1016/S0034-4257(01)00228-0).
- Næsset, E., Bollandsås, O.M., Gobakken, T., 2005. Comparing regression methods in estimation of biophysical properties of forest stands from two different inventories using laser scanner data. *Remote Sens. Environ.* 94, 541–553. <https://doi.org/10.1016/j.rse.2004.11.010>.
- Næsset, E., Gobakken, T., 2008. Estimation of above- and below-ground biomass across regions of the boreal forest zone using airborne laser. *Remote Sens. Environ.* 112, 3079–3090. <https://doi.org/10.1016/j.rse.2008.03.004>.
- Piao, S., Fang, J., Clais, P., Peylin, P., Huang, Y., Sitch, S., Wang, T., 2009. The carbon balance of terrestrial ecosystems in China. *Nature* 458, 1009. <https://doi.org/10.1038/nature07944>.
- Polewski, P., Yao, W., Cao, L., Gao, S., 2019. Marker-free coregistration of UAV and backpack LiDAR point clouds in forested areas. *ISPRS J. Photogramm. Remote Sens.* 147, 307–318. <https://doi.org/10.1016/j.isprsjprs.2018.11.020>.
- Reitberger, J., Schnörr, C., Krzystek, P., Stilla, U., 2009. 3D segmentation of single trees exploiting full waveform LiDAR data. *ISPRS J. Photogramm. Remote Sens.* 64, 561–574. <https://doi.org/10.1016/j.isprsjprs.2009.04.002>.
- Richardson, J.J., Moskal, L.M., Kim, S.H., 2009. Modeling approaches to estimate effective leaf area index from aerial discrete-return LiDAR. *Agric. For. Meteorol.* 149, 1152–1160. <https://doi.org/10.1016/j.agrformet.2009.02.007>.
- Sankey, T., Donager, J., McVay, J., Sankey, J.B., 2017. Uav lidar and hyperspectral fusion for forest monitoring in the southwestern USA. *Remote Sens. Environ.* 195, 30–43. <https://doi.org/10.1016/j.rse.2017.04.007>.
- Schomaker, M.E., Zarnoch, S.J., Bechtold, W.A., Latelle, D.J., Burkman, W.G., Cox, S.M., 2007. Crown-condition Classification: a Guide to Data Collection and Analysis. Gen. Tech. Rep. SRS-102: US Department of Agriculture, Forest Services.
- Shao, G., Shao, G., Gallion, J., Saunders, M.R., Frankenberger, J.R., Fei, S., 2018. Improving Lidar-based aboveground biomass estimation of temperate hardwood forests with varying site productivity. *Remote Sens. Environ.* 204, 872–882. <https://doi.org/10.1016/j.rse.2017.09.011>.
- Solberg, S., Næsset, E., Bollandsås, O.M., 2006. Single tree segmentation using airborne laser scanner data in a structurally heterogeneous spruce forest. *Photogramm. Eng. Remote Sensing* 72, 1369–1378. <https://doi.org/10.14358/pers.72.12.1369>.
- Straub, C., Weinacker, H., Koch, B., 2010. A comparison of different methods for forest resource estimation using information from airborne laser scanning and CIR orthophotos. *Eur. J. For. Res.* 129, 1069–1080. <https://doi.org/10.1007/s10342-010-0391-2>.
- Tao, S., Wu, F., Guo, Q., Wang, Y., Li, W., Xue, B., Hu, B., Li, P., Tian, D., Li, C., Yao, H., Li, Y., Xu, G., Fang, J., 2015. Segmenting tree crowns from terrestrial and mobile LiDAR data by exploring ecological theories. *ISPRS J. Photogramm. Remote Sens.* 110, 66–76. <https://doi.org/10.1016/j.isprsjprs.2015.10.007>.
- Thomas, V., Treitz, P., McCaughey, J.H., Morrison, I., 2006. Mapping stand-level forest biophysical variables for a mixedwood boreal forest using lidar: an examination of scanning density. *Can. J. For. Res.* 36, 34–47. <https://doi.org/10.1139/x05-230>.
- Van Leeuwen, M., Nieuwenhuis, M., 2010. Retrieval of forest structural parameters using LiDAR remote sensing. *Eur. J. For. Res.* 129, 749–770. <https://doi.org/10.1007/s10342-010-0381-4>.
- Wang, C., 2006. Biomass allometric equations for 10 co-occurring tree species in Chinese temperate forests. *For. Ecol. Manage.* 222, 9–16. <https://doi.org/10.1016/j.foreco.2005.10.074>.
- Wang, H., Pu, R., Zhu, Q., Ren, L., Zhang, Z.Z., 2015a. Mapping Health Levels of *Robinia pseudoacacia* Forests in the Yellow River Delta, China, Using IKONOS and Landsat 8 OLI Imagery. *Int. J. Remote Sens.* 36, 1114–1135. <https://doi.org/10.1117/j.jrs.10.045022>.
- Wang, H., Zhao, Y., Pu, R., Zhang, Z., 2015b. Mapping *Robinia pseudoacacia* Forest

- Health Conditions by Using Combined Spectral, Spatial, and Textural Information Extracted from IKONOS Imagery and Random Forest Classifier. *Remote Sens. (Basel)* 7, 9020–9044. <https://doi.org/10.3390/rs70709020>.
- Wang, H., Lu, K., Pu, R., 2016. Mapping Robinia pseudoacacia Forest Health in the Yellow River Delta by Using High-Resolution IKONOS Imagery and Object-Based Image Analysis. *J. Appl. Remote Sens.* 10, 045022. <https://doi.org/10.1117/1.JRS.10.045022>.
- Wang, H., Zhong, Y., Pu, R., Zhao, Y., Song, Y., Li, G., 2018. Dynamic analysis of Robinia pseudoacacia forest health levels from 1995 to 2013 in the Yellow River Delta, China using multitemporal Landsat imagery. *Int. J. Remote Sens.* 39, 4232–4253. <https://doi.org/10.1080/01431161.2018.1455236>.
- Weishampel, J.F., Drake, J.B., Cooper, A., Blair, J.B., Hofton, M., 2007. Forest canopy recovery from the 1938 hurricane and subsequent salvage damage measured with airborne LiDAR. *Remote Sens. Environ.* 109, 142–153. <https://doi.org/10.1016/j.rse.2006.12.016>.
- Wieser, M., Mandlbürger, G., Hollaus, M., Otepka, J., Glira, P., Pfeifer, N., 2017. A case study of UAS borne laser scanning for measurement of tree stem diameter. *Remote Sens. (Basel)* 9, 1154. <https://doi.org/10.3390/rs9111154>.
- Wu, J., Cawse-Nicholson, K., van Aardt, J., 2013. 3D Tree reconstruction from simulated small footprint waveform lidar. *Photogrammetric Eng. Remote Sensing.* 79, 1147–1157. <https://doi.org/10.14358/pers.79.12.1147>.
- Yoga, S., Bégin, J., St-Onge, B., Gatzliolis, D., 2017. Lidar and multispectral imagery classifications of balsam fir tree status for accurate predictions of merchantable volume. *Forests* 8, 253. <https://doi.org/10.3390/f8070253>.
- You, H., Wang, T., Skidmore, A., Xing, Y., 2017. Quantifying the effects of normalisation of airborne LiDAR intensity on coniferous forest leaf area index estimations. *Remote Sens.* 9, 163. <https://doi.org/10.3390/rs9020163>.
- Yu, X., Hyypä, J., Vastaranta, M., Holopainen, M., Viitala, R., 2011. Predicting individual tree attributes from airborne laser point clouds based on the random forests. *ISPRS J. Photogramm. Remote Sens.* 66, 28–37. <https://doi.org/10.1016/j.isprsjprs.2010.08.003>.
- Zhang, J., 2013. Strategies for Reclaiming and Ameliorating Saline Soil in the Yellow River Delta Region. Coastal Saline Soil Rehabilitation and Utilization Based on Forestry Approaches in China, Dobing Enterprises, Canada, 18 November. pp. 55–64. https://doi.org/10.1007/978-3-642-39915-2_7.
- Zhang, Z., Cao, L., She, G., 2017. Estimating forest structural parameters using canopy metrics derived from airborne LiDAR data in subtropical forests. *Remote Sens.* 9, 940. <https://doi.org/10.3390/rs9090940>.
- Zhao, K., Popescu, S., Nelson, R., 2009. Lidar remote sensing of forest biomass: a scale-invariant estimation approach using airborne lasers. *Remote Sens. Environ.* 113, 182–196. <https://doi.org/10.1016/j.rse.2008.09.009>.
- Zhao, X., Guo, Q., Su, Y., Xue, B., 2016. Improved progressive TIN densification filtering algorithm for airborne LiDAR data in forested areas. *ISPRS J. Photogramm. Remote Sens.* 117, 79–91. <https://doi.org/10.1016/j.isprsjprs.2016.03.016>.
- Zhen, Z., Quackenbush, L.J., Zhang, L.J., 2016. Trends in automatic individual tree crown detection and delineation-evolution of LiDAR data. *Remote Sens.* 8, 333. <https://doi.org/10.3390/rs8040333>.
- Zheng, G., Chen, J.M., Tian, Q.J., Ju, W.M., Xia, X.Q., 2007. Combining remote sensing imagery and forest age inventory for biomass mapping. *J. Environ. Manag.* 85, 616–623. <https://doi.org/10.1016/j.jenvman.2006.07.015>.
- Zhou, D., Zhao, S., Zhu, C., 2012. The Grain for Green Project induced land cover change in the Loess Plateau: A case study with Ansai County, Shanxi Province, China. *Ecol. Indic.* 23, 88–94. <https://doi.org/10.1016/j.ecolind.2012.03.021>.